The aerodynamics of floating offshore wind turbines in different working states during surge motion

Dong, Jing; Viré, Axelle

DOI
10.1016/j.renene.2022.06.016

Publication date
2022

Document Version
Final published version

Published in
Renewable Energy

Renewable Energy 195 (2022) 1125–1136

Contents lists available at ScienceDirect

Renewable Energy

journal homepage: www.elsevier.com/locate/renene

The aerodynamics of floating offshore wind turbines in different working states during surge motion

Jing Dong [a, b, *], Axelle Viré [a]

[a] Wind Energy Section, Delft University of Technology, Delft, the Netherlands
[b] Institute of Civil and Environmental Engineering, Norwegian University of Science and Technology, Trondheim, Norway

ARTICLE INFO

Article history:
Received 12 May 2021
Received in revised form
2 June 2022
Accepted 4 June 2022
Available online 13 June 2022

Keywords:
Vortex ring state (VRS)
Rotor-wake interaction
Floating offshore wind turbine (FOWT)
Free wake vortex method
Wind energy
Aerodynamics

ABSTRACT

The rotor of floating offshore wind turbines with platform motions may undergo different working states during its operation, e.g. from windmill working state to vortex ring and propeller working state. In this paper, an aerodynamic model based on a free wake vortex method is used to simulate the rotor undergoing surge motion. The associated change of working states of the rotor is evaluated quantitatively and visually. The results show that during a full cycle of the surge motion of the floating platform, the rotor experiences alternative onset of the windmill state, vortex ring state, and propeller state, while the later two occur only during the downwind motion of the rotor. The aerodynamic load change corresponding to different working states of the rotor indicates that the vortex ring state is the most unstable phase of the three.

1. Introduction

Floating offshore wind turbines (FOWTs) often undergo large platform motions that have significant influence on aerodynamic loads of the rotor, and may lead to changes of the rotor working states. According to different levels of blade-wake interactions, there exist four different working states of a wind turbine rotor [1]: windmill working state, turbulence working state, vortex ring state (VRS), and propeller working state (PWS), as shown Fig. 1. When the wind turbine operates in the windmill working state, it extracts energy from the wind and the flow forms a clear stream tube around the rotor. This is the most common situation for wind turbines placed on fixed foundations, both onshore and offshore. In the turbulent wake state the rotor interacts with unsteady flow and the momentum balance equations begin to break down [1]; the vortex ring state, the rotor strongly interacts with its own wake and the rotor is subjected to flow reversal. The flow and loads are highly unsteady. Finally, during the propeller working state, the flow stream is reversed and the wind turbine adds kinetic energy to the flow like a propeller. This paper focuses on the change of working state during the surge motion of a floating offshore wind turbine with steady free stream wind conditions.

The motion of FOWTs is a dynamic process, whereby the wind turbine rotor periodically interacts with its own wake. In that case, the stream tube around the rotor may break down, and the vortex ring state and propeller working state may occur. The VRS phenomenon was first discovered on helicopters, which was considered to be a serious safety problem for the flight [2]. The possible existence of the VRS for FOWTs was first introduced by Sebastian [1] in 2013. And then some numerical simulations are done [3–6] which shew the existence of the VRS on FOWTs as a real-world problem. The study of the VRS on both FOWTs and helicopters show that the onset of the vortex ring state may cause the following aerodynamic problems to the rotor [2,4–6]. First, the rotation becomes apparently unsteady and aperiodic. Then the blades experience successive forward and backward velocities, which can lead to significant blade flapping and a loss of rotor control. Finally, the level of thrust fluctuations is high, which may cause trouble to the control system of the wind turbine.

In the context of FOWTs, it was shown that the vortex ring state is followed by the propeller state, during which the rotor inputs kinetic energy into the flow [3]. The research on these specific working states of a FOWT is still limited. However, with the development of the offshore wind energy technology and the

* Corresponding author. Wind Energy Section, Delft University of Technology, Delft, the Netherlands.
E-mail addresses: j.dong-2@tudelft.nl, dj0116@163.com (J. Dong).

https://doi.org/10.1016/j.renene.2022.06.016

Acronyms

FOWT	Floating Offshore Wind Turbine
VRS	Vortex Ring State
PWS	Propeller Working State
BEM	Blade Element Momentum Theory
CFD	Computational Fluid Dynamics
FWVF	Free Wake Vortex Filament Method
NVLM	Nonlinear Vortex Lattice Method
FWVR	Free Wake Vortex Ring Method

commercialization process of floating wind turbines, the understanding of the vortex ring state and the propeller working state is becoming increasingly important.

In order to simulate these rotor-wake interaction problems in the context of FOWTs, both the platform motion and the rotor aerodynamics need to be considered simultaneously, which requires an aero-hydro coupled analysis. For the sake of reducing the computational time of such analyses, low- or mid-fidelity tools are often adopted. So far, the coupled analysis tools are almost exclusively based on the blade element momentum (BEM) theory, which describes the steady state behavior of a wind turbine but may be unsuitable when the rotor strongly interacts with its own wake, as it is the case for the VRS. By contrast, various vortex based methods are developed and can deal with the aerodynamic calculation of wind turbine rotors undergoing a prescribed motion. For example, the wake structure of FOWTs has been analyzed using a free wake vortex filament (FWVF) method [7], vortex particles such as the nonlinear vortex lattice method (NVLM) [8], and free wake vortex ring (FWVR) models [9–11]. Also, Jeon [12] used a vortex lattice method for the unsteady aerodynamics of FOWTs subjected to platform pitching motion. Higher fidelity tools such as computational fluid dynamics (CFD) can also be used to investigate rotor-wake interaction problems, although they are much more time consuming. For example, Tran [13,14] studied the unsteady aerodynamics FOWTs using a CFD model. Recently, Kyle [3] also used a CFD model to simulate the surge motion of a FOWT under rated and below rated wind speeds, and showed the existence of the propeller working state and the vortex ring state during the floater motion. In this research, the propeller working state is identified when the thrust coefficient and the relative velocity at the rotor become negative. During VRS, blade tip-vortex interaction and root vortex recirculation with a negative relative rotor velocity were observed. In some of our earlier studies [4,5], criteria from the helicopter research community [15,16] were modified in order to identify the occurrence of VRS for FOWTs. In these works, the VRS boundaries were predicted using an aero-hydro coupled analysis for FOWTs undergoing joint wave/wind loads. Furthermore, the dramatic change of the aerodynamic performance of the rotor was found to be mostly due to the platform motion rather than the induction from the wake.

The objectives of this paper are to captured the working state changes of the FOWT, identifying boundaries between different working states and analyzing the aerodynamic characteristic of the wind turbine during working state changes. In order to do so, a free wake vortex ring method [11] is used to simulate the wind turbine rotor dynamics under a prescribed surge motion. The following research questions are addressed.

1. With the vortex model, can we capture the propeller working state after the onset of the vortex ring state, as indicated the CFD analysis from Kyle [3]?
2. How can the boundaries between the propeller working state and the vortex ring state be identified?
3. What is the influence of the change of working states on the aerodynamic performance of the rotor?

2. Vortex theory

A vortex based method called free wake vortex ring method [11] is used to build up the aerodynamic model for the simulation of the rotor-wake interaction problem in this research. The vortex theory of this aerodynamic model for a moving rotor is briefly introduced here.

2.1. The vortex filament induced velocity based on Biot-Savart law

The Biot–Savart law is used in aerodynamic theory to calculate the velocity induced by various vortex elements including vortex filament, vortex particle and so on. Considering a vortex filament $C(q)$ with a constant strength Γ, the induced velocity $\mathbf{V}_P$ in a field Ξ at a point P can be expressed by Biot-Savart law as [17].

$$\mathbf{V}_P = \Gamma \int_{C(q)} \mathbf{K}_\sigma(\mathbf{r}) \times \frac{\partial \mathbf{r}_q}{\partial q} dq, \tag{1}$$

where $\mathbf{K}_\sigma(\mathbf{r})$ is the desingularized kernel of Biot-Savart operator. Denoting $\mathbf{r}_P$ as the position vector of point P, $\mathbf{r}_q$ as the position vector of a point Q on the filament, $\mathbf{r} = \mathbf{r}_P - \mathbf{r}_q$ is the vector pointing from the point Q to point P, and $\frac{\partial \mathbf{r}_q}{\partial q}$ is the partial derivative on the filament which represents the tangential direction along $C(q)$.

Considering the induced velocity of a straight line vortex filament on a field point P, as shown in Fig. 2, the parametric curve of the vortex filament is $\mathbf{C}(q) = \mathbf{x}_1 + q(\mathbf{x}_2 - \mathbf{x}_1)$, where $0 \le q \le 1$, thus the desingularized kernel $\mathbf{K}_\sigma(\mathbf{r})$ can be expressed as

$$\begin{aligned} \mathbf{K}_\sigma(\mathbf{r}) &= -\frac{\mathbf{x}_P - \mathbf{C}(q)}{4\pi(|\mathbf{x}_P - \mathbf{C}(q)|^2 + r_c^2)^{\frac{3}{2}}} \\ &= -\frac{\mathbf{x}_P - (1-q)\mathbf{x}_1 + q\mathbf{x}_2}{4\pi(|\mathbf{x}_P - (1-q)\mathbf{x}_1 + q\mathbf{x}_2|^2 + r_c^2)^{\frac{3}{2}}}. \end{aligned} \tag{2}$$

where r_c is the vortex core radius. Accordingly, the induced velocity

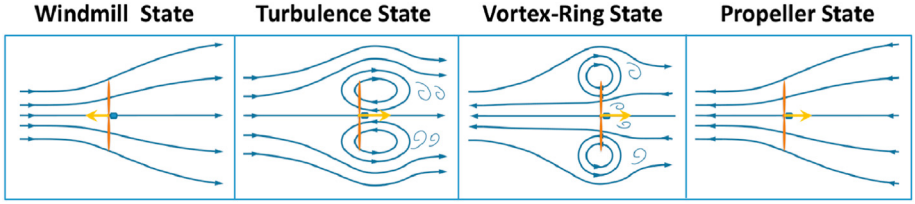

Fig. 1. Four working states of FOWTs.

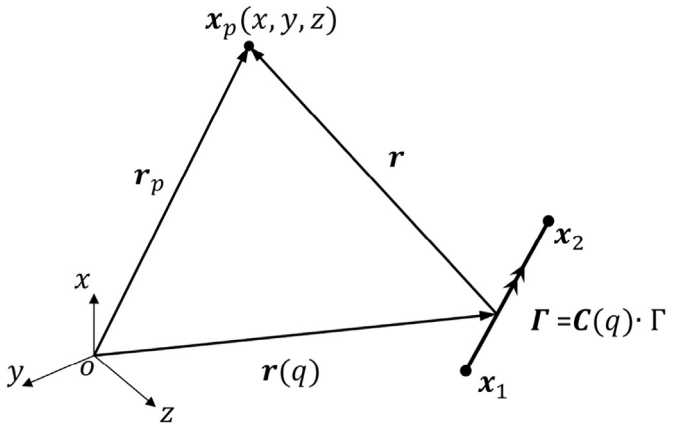

Fig. 2. Straight line vortex induced velocity.

$\mathbf{V}_P$ can be expressed as

$$\mathbf{V}_P = -\Gamma\int_0^1 \frac{\mathbf{x}_P-(1-q)\mathbf{x}_1+q\mathbf{x}_2}{4\pi(|\mathbf{x}_P-(1-q)\mathbf{x}_1+q\mathbf{x}_2|^2+r_c^2)^{\frac{3}{2}}}\times(\mathbf{x}_2-\mathbf{x}_1)dq. \tag{3}$$

2.2. The vortex ring induced velocity

Considering an ideal vortex ring with radius R as shown in Fig. 3, its parametric curve $C(\chi)$ with the angle χ as the parametrisation parameter can be expressed as

$$C(\chi) = R(\cos\chi, \sin\chi, 0), \qquad \chi\in[0, 2\pi). \tag{4}$$

Since the vortex ring is axis-symmetric, its local vortex ring coordinate system xyz can be adjusted according to the location of the field point P, thereby the field point P can be put into the top half of xz-plane with the coordinate $(x_P, 0, z_P)$ while $C(\chi)$ is in the xy-plane at the origin of the z-axis. Thus, taking the notation $x_P = \eta R$ and $z_P = \zeta R$, the coordinate of the field point P can be expressed as

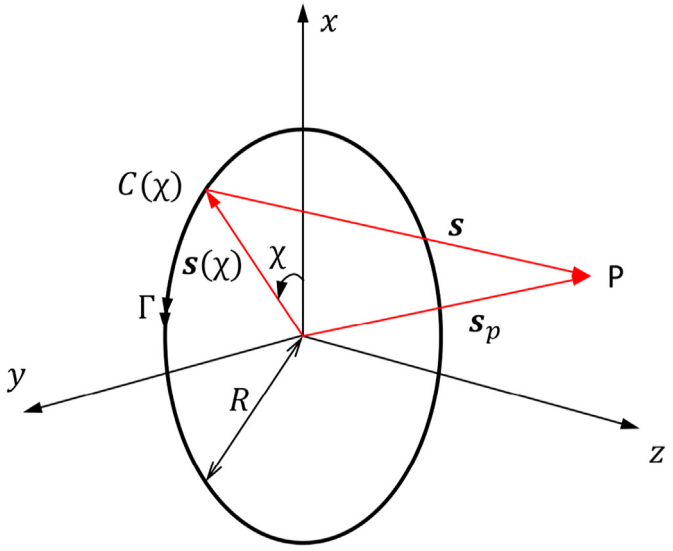

Fig. 3. Vortex ring coordinate system.

$$\mathbf{P} = R(\eta, 0, \zeta), \qquad \eta\in(0, +\infty), \zeta\in(-\infty, +\infty). \tag{5}$$

Accordingly, $\mathbf{r}(\chi)$ and $\mathbf{r}_P$ can be expressed as

$$\mathbf{r}(\chi) = R(\cos\chi, \sin\chi, 0), \tag{6}$$

$$\mathbf{r}_P = R(\eta, 0, \zeta). \tag{7}$$

Thus the displacement vector $\mathbf{r}$ can be expressed as

$$\begin{aligned}\mathbf{r} &= \mathbf{r}_P - \mathbf{r}(\chi)\\ &= R(\eta-\cos\chi, -\sin\chi, \zeta).\end{aligned} \tag{8}$$

Substituting equations (4) and (6-8) into equation (1) yields the following vortex ring induced velocity $\mathbf{V}$ at point P,

$$\mathbf{V} = -\frac{\Gamma}{4\pi R}\int_0^{2\pi}\frac{(\zeta\cos\chi, \zeta\sin\chi, 1-\eta\cos\chi)}{(1+\eta^2+\zeta^2+\sigma^2-2\eta\cos\chi)^{\frac{3}{2}}}d\chi, \tag{9}$$

where $\sigma = \frac{r_c}{R}$ is the non-dimensional core radius of the vortex filament. An analytical result of this integral has been derived as below [18,19].

$$V_x = \frac{\Gamma}{2\pi R C_0}\left[-K(m) + \frac{1+\eta^2+\zeta^2}{C_1^2}E(m)\right]\frac{\zeta}{\eta}, \tag{10}$$

$$V_z = \frac{\Gamma}{2\pi R C_0}\left[K(m) + \frac{1-\eta^2-\zeta^2}{C_1^2}E(m)\right]. \tag{11}$$

and

$$C_0^2 = 1+2\eta+\eta^2+\zeta^2+\sigma^2, \tag{12}$$

$$C_1^2 = 1-2\eta+\eta^2+\zeta^2+\sigma^2. \tag{13}$$

The functions $K(m)$ and $E(m)$ are the first and second type of complete elliptic integrals respectively. The item m is the elliptic parameter defined as:

$$m = \frac{4\eta}{C_0^2}. \tag{14}$$

An in-house code based on the free wake vortex ring method [11] is used to simulate the rotor-wake interaction problem. The method includes two parts: the near wake model and the far wake model. The near wake model is represented by finite length vortex filaments both bounded on and trailed from the blades, while the far wake model is represented by the vortex ring elements as introduced in Dong et al. [11].

It is worth mention that the near wake model is perpendicular to the rotor axis and does not induce velocity in the rotor plane. The far wake vortex rings induce velocities in directions according to their own position. Thus the rotational induction factor cannot be simulated accurately due to the limitation of the model itself.

3. Criteria for the VRS prediction

Two criteria are used in this paper to predict the occurrence of VRS: the axial induction factor 'a' and the Wolkovitch criterion 'w'.

3.1. Criterion 1

The axial induction factor a defined in the rotor-fixed reference

frame is defined as

$$a = \frac{V_I}{(V_\infty - V_p)}, \tag{15}$$

where V_∞ is the free-stream velocity, V_I is the induced velocity at the rotor and V_p is the velocity of the platform motion. This equation can also be written as:

$$V_{rel} = (V_\infty - V_p)(1 - a), \tag{16}$$

where V_{rel} is the axial relative velocity at the rotor. Equation (16) is written in a form that explicitly shows that when $a = 1$, $V_{rel} = 0$, which means the rotor has the same velocity with its wake. Thus, the value $a \geq 1$ is taken as a benchmark to research the VRS.

3.2. Criterion 2

Wolkovitch criterion [15] uses the momentum theory and actuator disk concept to predict the occurrence of the vortex ring state. As shown in Fig. 4, $\mathbf{V}_R$ is the relative wind velocity to the actuator disc, $\mathbf{V}_I$ is the induced velocity at the rotor disc and α is the angle between $\mathbf{V}_R$ and the actuator disc. The rotor is assumed to be surrounded by a vortex tube, inside of which the flow is uniform at any cross section. Outside the tube, the wind speed equals the relative value. This vortex tube is formed of a series of vortex cores. Thus, near the rotor and outside of the tube, the leeward component of the stream velocity is $\mathbf{V}_R \sin\alpha$, while inside the tube the windward velocity component is $(\mathbf{V}_I - \mathbf{V}_R \sin\alpha)$. The velocity of the vortex core center is the average between these velocities, i.e. $(\mathbf{V}_I/2 - \mathbf{V}_R \sin\alpha)$, and points in the leeward direction. The vortex ring state is assumed to occur when the relative velocity of the vortex cores normal to the rotor disc falls to zero. Thus the critical velocity V_{crit} associated with Wolkovitch's criterion is given by

$$V_{crit} = \frac{V_I}{2\sin\alpha}. \tag{17}$$

This means that when the velocity is smaller than the critical velocity, the rotor is in a vortex ring state. Wolkovitch's criterion is considered to predict the VRS when the rotor enters the center of the vortex ring.

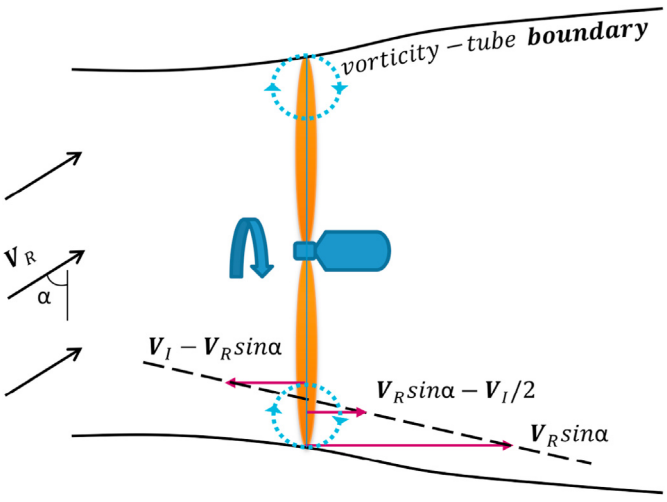

Fig. 4. Illustration of a stream tube and components of the wind speed in the context of the Wolkovitch's model.

4. Load case design for NREL 5 MW reference turbine

4.1. NREL 5 MW reference turbine

The same load cases as given in the literature [3] are adopted here, and relate to the NREL 5 MW reference wind turbine [20] with a 5° shaft tilt angle. The basic turbine parameters shown in Table 1. Two reference coordinate systems are used in the analysis: the inertial reference coordinate system S' and the rotor-fixed reference coordinate system S'', as shown in Fig. 5.

The inertial reference coordinate system is defined as:

- The origin S' fixing on the Earth.
- x' axis pointing vertically upward opposite to gravity.
- y' axis pointing to the right when looking in the nominal downwind direction.
- z' axis pointing in the nominal (0°) downwind direction.

The rotor-fixed reference coordinate system is defined as:

- The origin fixing on the rotor center S'', translating and rotating with the wind turbine tower.
- x'' axis orthogonal with the y'' and z'' axes such that they form a right-handed coordinate system.
- y'' axis pointing to the right when looking from the tower towards the nominally downwind end of the nacelle.
- z'' axis pointing along the (possibly tilted) shaft in the nominally downwind direction.

The inertial reference coordinate system is applied when describing the platform motions and the rotor motions, while the rotor-fixed reference coordinate system is applied when describing the flow field around the rotor and the load perceived by the rotor.

4.2. Load cases description

In order to capture the VRS and PWS during a pure surge motion of the rotor, a below-rated wind speed of 7 m/s was investigated both with and without prescribed surge motion [3], as summarized in Table 2. The load cases are labeled as: BF and BS, where 'B' represents 'Below' rated wind speed, 'F' represents 'Fixed' and 'S' represents 'Surge'. V_∞ is the free stream velocity and A_s is the amplitude of the sinusoidal surge motion. Accordingly, the surge displacement, χ_s, is defined as:

$$\chi_s = A_s \sin(\omega_s t), \tag{18}$$

where ω_s is the surge frequency in rad/s and t is time in seconds. And the surge velocity of the rotor is identified as:

$$u_s = \frac{d\chi_s}{dt} = A_s \omega_s \cos(\omega_s t). \tag{19}$$

The original design of this set of load cases is formulated

Table 1
Characteristics of the NREL 5 MW reference turbine.

Rating	5 MW
Rotor Orientation, Configuration	Upwind, 3 Blades
Rotor, Hub Diameter	126 m, 3 m
Cut-In, Rated, Cut-Out Wind Speed	3 m/s, 11.4 m/s, 25 m/s
Cut-In, Rated Rotor Speed	6.9 rpm, 12.1 rpm
Rated Tip Speed	80 m/s
Overhang, Shaft Tilt, Precone	5 m, 5°, 2.5°
Coordinate Location of Overall CM	(-0.2 m, 0.0 m, 64.0 m)

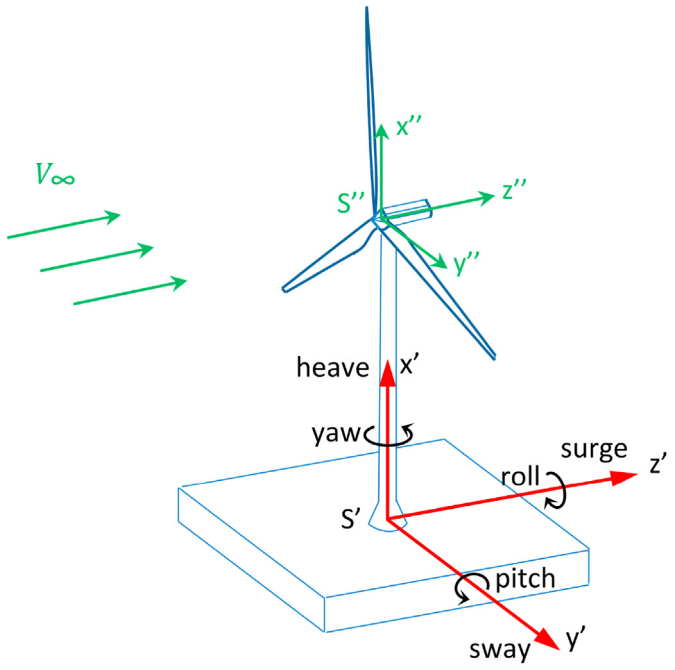

Fig. 5. Inertial reference system and rotor-fixed reference system.

Table 2
Rated and below-rated load cases.

Lable	Rotation rate [rpm]	V_∞ [m/s]	A_s [m]	Surge period [s]
BF	8.47	7.0	–	–
BS	8.47	7.0	9.4	8.1

according to the response amplitude operators (RAO) which predicts the surge motion of the whole wind system, with the assumption that the 5 MW NREL reference wind turbine is mounted on a barge platform. The translational RAO is defined as:

$$RAO_i(\omega) = \left|\frac{\Xi_i(\omega)}{A_{wave}}\right| \quad i = 1, 2, 3, \tag{20}$$

where ω is the wave frequency, Ξ is the system response amplitude, A_{wave} is the wave amplitude, and $i = 1, 2, 3$ corresponding to surge, heave and sway, respectively. The barge surge RAO amplitude is taken as 5. In order to get a VRS from a pure surge motion of the platform, the wave condition is set as follows: wave height $A_{wave} = 1.87m$ and wave period of $8.1s$. This leads to a platform surge amplitude of $9.4m$ and surge period of $8.1s$ [3]. It is worth mentioning that the surge frequency is quite high, which leads to only a short period during the surge cycle for the onset and development of VRS. This surge period is much smaller than what is expected in reality for floating wind turbines. However, these values are identical to those investigated by Kyle et al. [3], and therefore, enable a direct comparison with their CFD results.

5. Results

Each load case has been simulated for 150 s, with a time step $\Delta t = 0.1968s$.

5.1. The boundaries between the windmill working state and the vortex ring state

In order to analyze the working state change in the whole cycle of the rotor motion, the VRS boundaries are first predicted for the load cases with surge motions according to the axial induction factor 'a' (yellow area) and the Wolkovitch criterion 'w' (blue area) respectively. The VRS boundaries in one cycle of the rotor surge motion (right axis) are shown in Fig. 6 and Fig. 7. The figures are plotted based on the results of one of the three blades of the rotor, horizontal axis represents the time line and the vertical axis represents the blade span. It can be seen that according to 'a', the duration of the VRS in this cycle is 2.1s (from 112.6s to 114.7s). While according to 'w', the duration of the VRS in this cycle is 2.6s (from 112.4s to 115.0s). Thus, the 'w' criterion covers a wider spatial and temporal range than the 'a' criterion.

5.2. Distinguish different working states in velocity field

The criteria outlined above are used to identify the VRS boundaries. In order to assess whether the propeller working state (PWS) occurs, the velocity fields around the rotor are further examined. This is done by plotting the velocity fields around the rotor, in a longitudinal section in the center plane of the rotor in the rotor-fixed reference frame. In these plots, the horizontal axis points downwind and the vertical axis points upward (both have the unit of [m]), and the rotor position is marked with a black line. Firstly the velocity field of the fixed rotor 'BF' is plotted for reference, as shown in Fig. 8. The typical windmill state is observed with small velocity gradients in front of the rotor, a significant drop of velocity behind the rotor, and the stream lines expansion from the rotor downwind. In comparison, Figs. 9–19 show the velocity fields at different instants in the surge motion. From the shape of the stream lines and the contour plots of the relative velocity normal to the rotor, it can be seen that the velocity experienced by the rotor changes dramatically in a such short period of time. At 111.583s in Fig. 9, the rotor is in the windmill state, and then, at 111.977s in Fig. 10, the vortices begin to accumulate downstream. At 112.371s in Fig. 11 and 114.535s in Fig. 16, the vortices accumulate near the rotor and the velocities at the rotor are very small. At 112.567s in Figs. 12 and 114.339s in Fig. 15, the rotor are engulfed by the vortices and the velocity at the rotor changes sign, which clearly indicates that the rotor experiences VRS. At 113.158s in Figs. 13 and 113.551s in Fig. 14, the stream lines cross the rotor from downwind to upwind, which indicates that the rotor operates in the propeller working state (PWS). From 114.732s in Figs. 17 to 114.929s in Fig. 18,

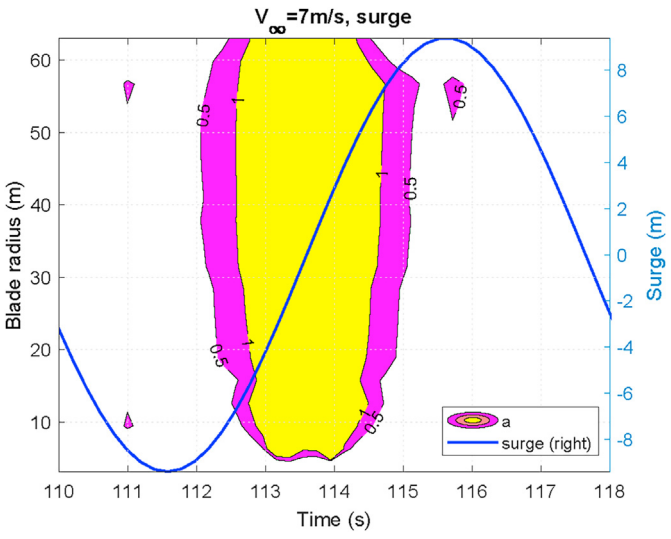

Fig. 6. The VRS predicted with 'a'.

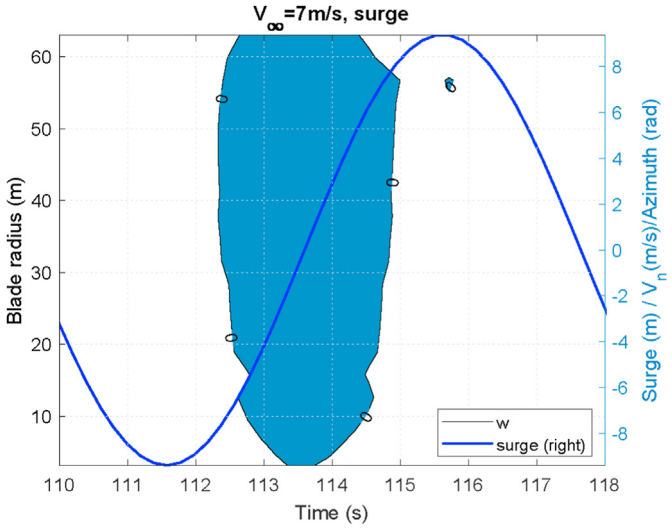

Fig. 7. The VRS predicted with 'w'.

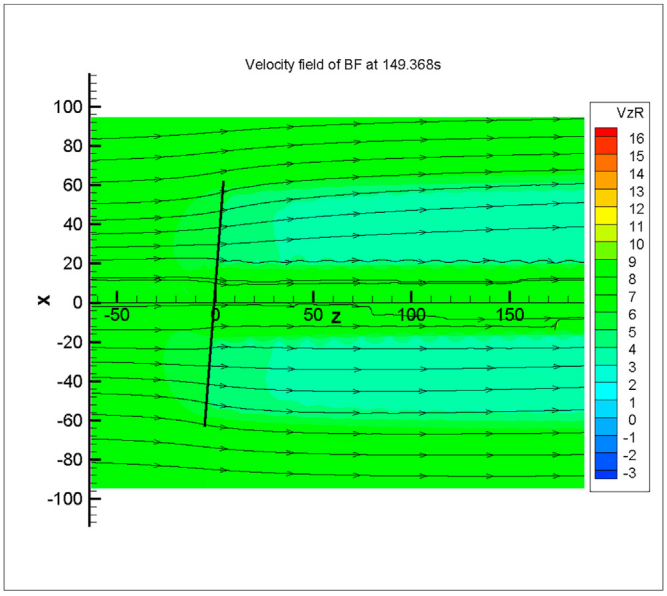

Fig. 8. The velocity field around the rotor at 149.368s (BF).

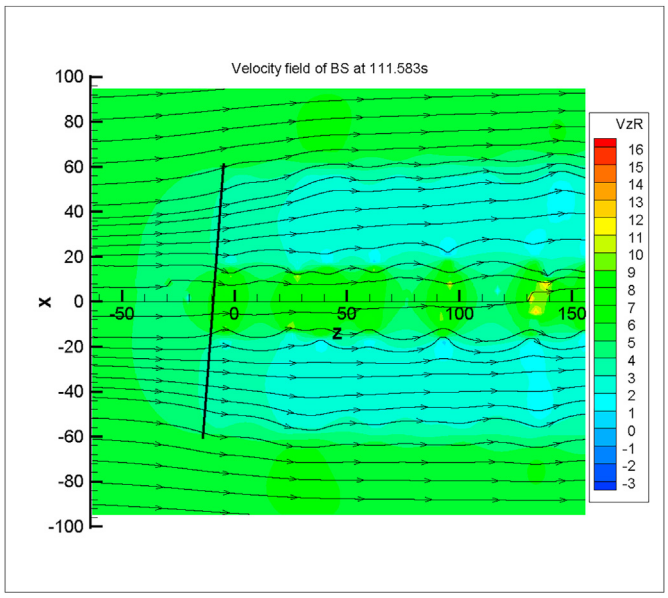

Fig. 9. The velocity field around the rotor at 111.583s (BS).

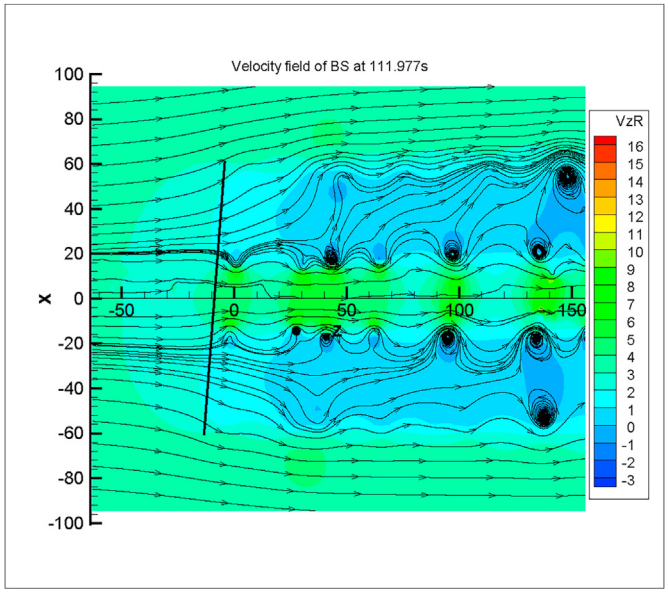

Fig. 10. The velocity field around the rotor at 111.977s (BS).

the rotor goes back to the windmill state. And at 117.487s in Fig. 19, the windmill working state with the highest velocity around the rotor is identified.

This analysis leads to the following observations. Firstly, in this load case, the sequence of working state in one cycle of the surge motion is: windmill working state, vortex ring state, propeller working state, vortex ring state again, and finally windmill working state. Secondly, the VRS itself is a dynamic process, where the vortices start to accumulate in the far wake, then near the rotor, with the rotor being engulfed by them, before the rotor moves away from them. Thirdly, the PWS is identified by the typical shape of the streamlines in this particular load case. But it is worth mentioning that the PWS does not necessarily always happen after the VRS. This depends on the actual relative velocity perceived by the rotor.

5.3. The boundaries between the propeller working state and vortex ring state according to angle of attack

From the above analysis it can be seen that in the typical VRS, the airflow goes upwind from the inboard of the blade and goes downwind from outboard of the blade. While in the typical PWS, the airflow goes upwind uniformly all along the blade. The airflow direction will significantly influence the angle of attacks (AoA), which give us a favorable condition to predict the boundary between the VRS and PWS quantitatively. Accordingly, the angles of attack (AOAs) denoted by α at different time steps are evaluated and compared with the negative twist angles denoted by $\theta_{-twist} = -\theta_t$, which represents the AoAs when the relative wind velocity

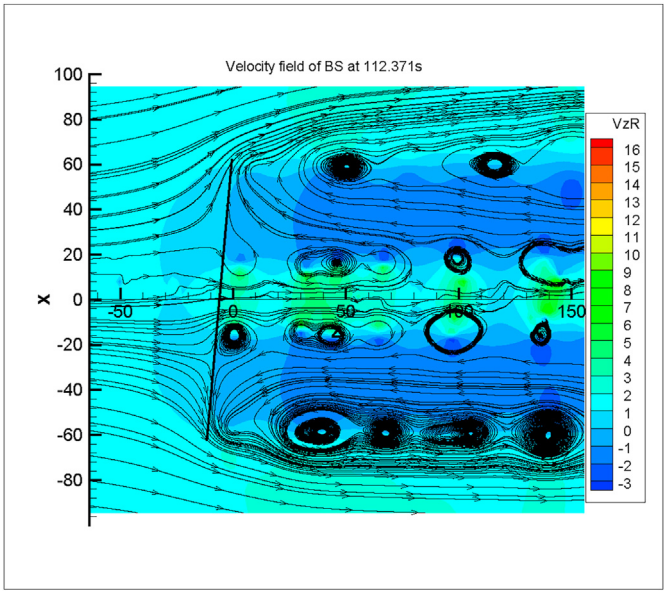

Fig. 11. The velocity field around the rotor at 112.371s (BS).

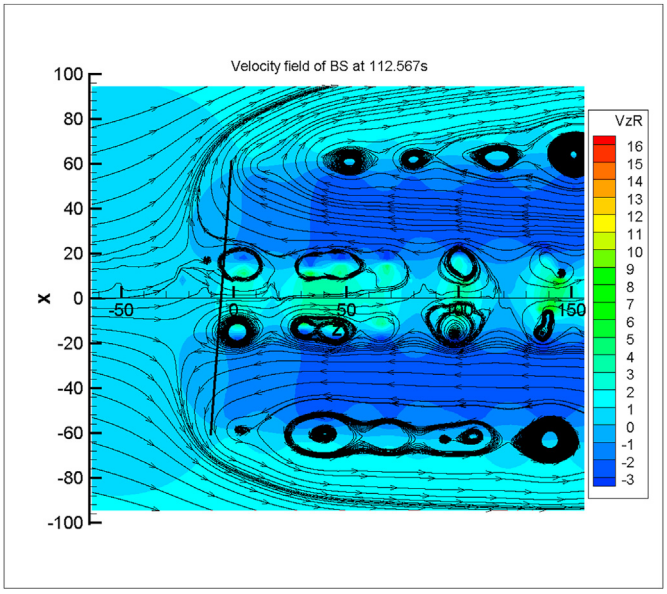

Fig. 12. The velocity field around the rotor at 112.567s (BS).

$V_0(1-a)$ is zero, assuming that the collective pitch angle θ_p of the blades is zero as illustrated in Fig. 20.

The values of AoAs along the blade in a time span from 111.780s to 115.126s are shown in Fig. 21, where it can be seen that with the working state changes from the windmill working state to the propeller working state as analyzed in Section 5.2, the AoAs along the blade gradually drop from positive to negative values. From 112.961s to 114.142s, the AoAs along the blade are well below the negative twist angles θ_{-twist}. Also, it can be noticed that the time instants corresponding to the onset of the PWS which can be visually identified in Figs. 13 and 14 exactly drop in this region when AoAs are smaller than θ_{-twist}. On the other hand, when the working state is visually seen as typical VRS as shown in Figs. 12 and 15, the AoA curve and the θ_{-twist} curve have intersections. Thus, it is concluded that the boundary between the VRS and PWS can be

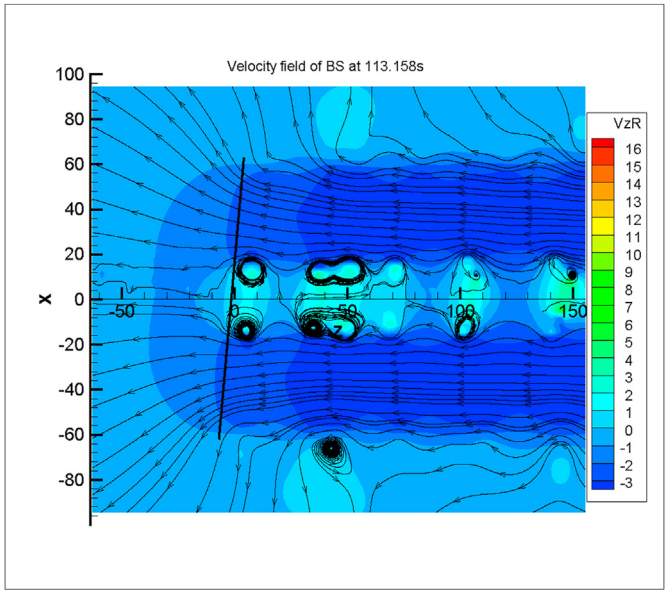

Fig. 13. The velocity field around the rotor at 113.158s (BS).

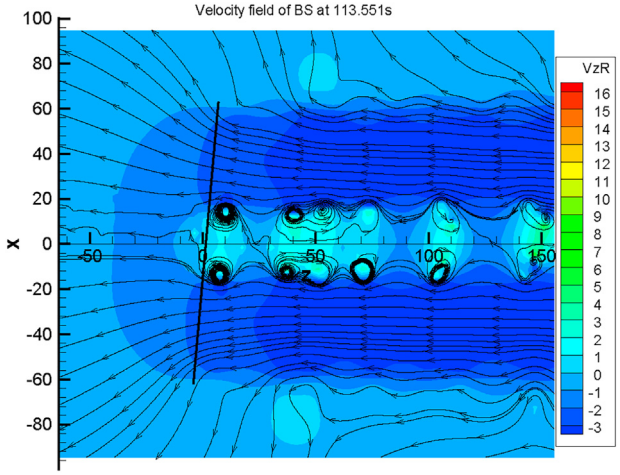

Fig. 14. The velocity field around the rotor at 113.551s (BS).

predicted in the condition when α becomes smaller than θ_{-twist} all along the blade. For this particular surge cycle of the load case 'BS', the boundaries between the VRS and PWS are identified at 112.961s and 114.142s.

5.4. Thrust coefficients corresponding to the working states of the rotor

The thrust coefficients on the rotor C_T is defined as

$$C_T = \frac{T_x}{0.5\rho_{air}A_{rotor}V_\infty}, \tag{21}$$

where T_x in the thrust in Newton which is normal to the rotor, ρ_{air} is the air density taken as 1.225 kg/m^3, A_{rotor} is the rotor swept area in m^2 and V_∞ is the free stream velocity in m/s.

The time evolution of the thrust coefficient within one period of the surge motion is plotted in Fig. 22, where the corresponding working states (as identified in Sections 5.1, 5.2 and 5.3) are also

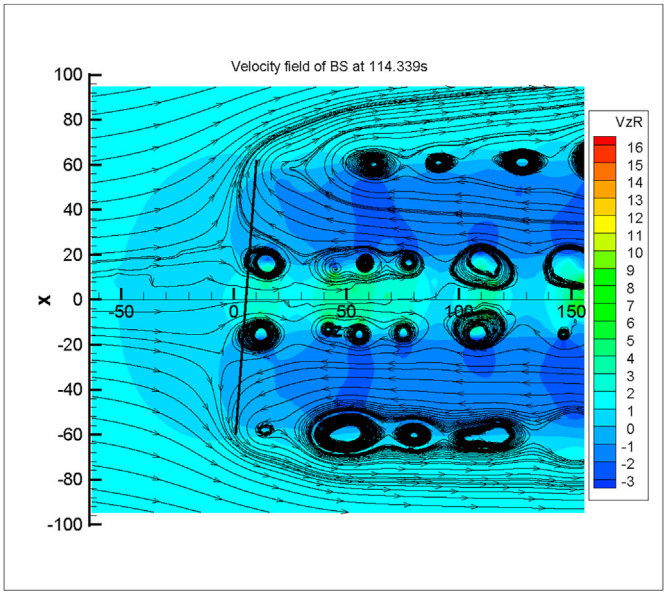

Fig. 15. The velocity field around the rotor at 114.339s (BS).

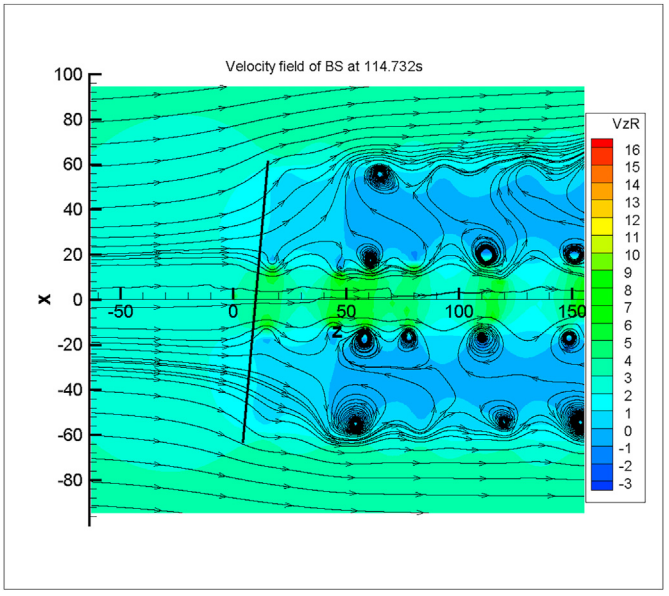

Fig. 17. The velocity field around the rotor at 114.732s (BS).

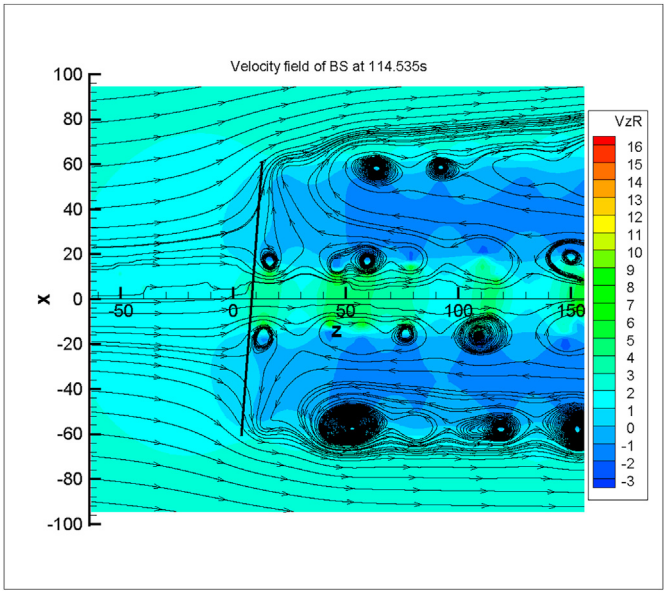

Fig. 16. The velocity field around the rotor at 114.535s (BS).

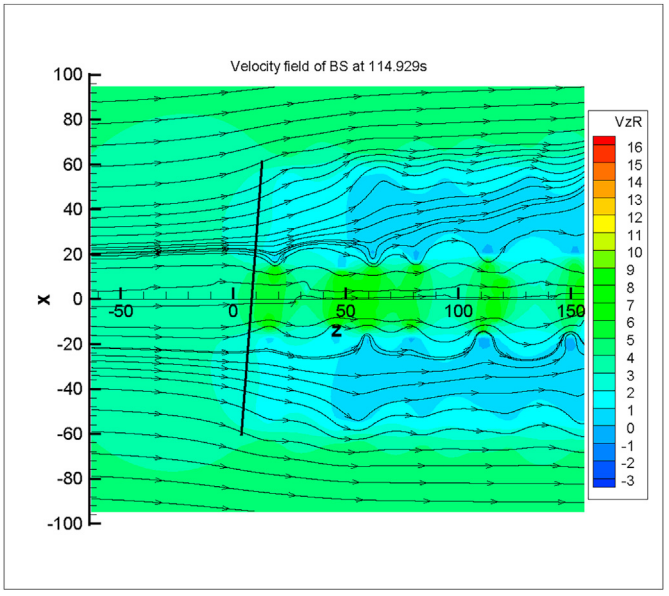

Fig. 18. The velocity field around the rotor at 114.929s (BS).

shown. In the figure, a stands for the axial induction factor, while w1 and w2 represent the boundaries between windmill working state and the VRS according to Wolkovitch criterion; and P1, P2 represent the boundaries between the VRS and PWS. The time instants of $a = 0.5$ and $a = 1$ are taken from the boundaries of the purple region and the yellow region on both side of Fig. 6 respectively. The time instants of w1 and w2 are taken from the boundaries of the blue region on both side of Fig. 7. And the time instants of P1 and P2 are identified according to the relationship of the angle of attack and the negative twist angle as shown in Fig. 21.

The regions dominated by the windmill working state, VRS and PWS, respectively, are marked in the figure. It can be seen that, in this load case, the rotor works in the windmill state for most of the time. However, the VRS occurs when C_T is positive (according to either the criterion 'a' or 'w') and extends until C_T becomes negative, while the PWS occurs only when C_T is well below zero. It is also worth mentioning that the turbulent wake state did not occur in this simulation. We considered that the turbulent wake state didn't occur because based on the definition, the turbulent wake state corresponds to an increase of C_T. In this simulation, even though the chaotic flow around the rotor was observed, C_T didn't increase. This can be due to the fact that the vortex model is developed based on potential flow assumption without viscous effects and with low fidelity in terms of the modeling of blades. Thus, we suggest that to further verify this problem, CFD methods need to be used. Also due to that the surge motion of the rotor is imposed and the floater velocity regularly changes sign. The results of this study show that the VRS is not necessarily an outcome of the development of the turbulent wake state, but can appear directly after the windmill working state. However, higher-fidelity models

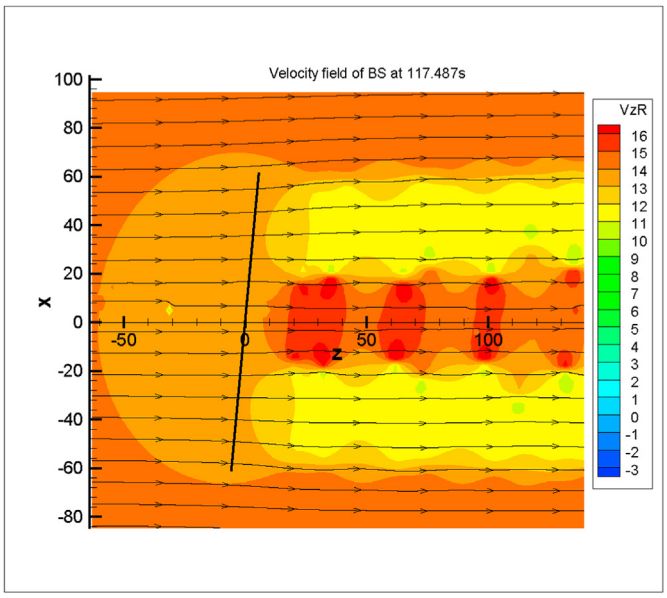

Fig. 19. The velocity field around the rotor at 117.487s (BS).

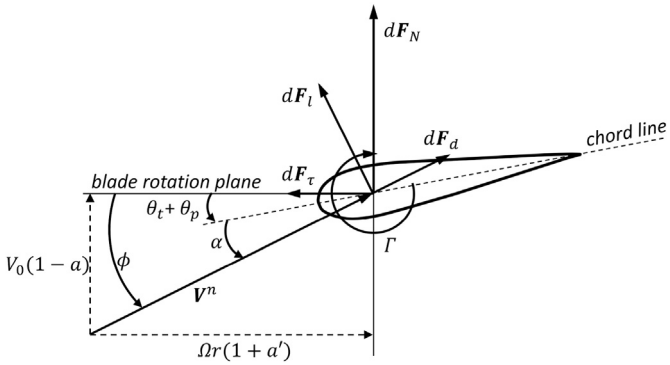

Fig. 20. Forces acting on a blade element [11].

that do not rely on the potential flow assumption should be used to confirm this observation.

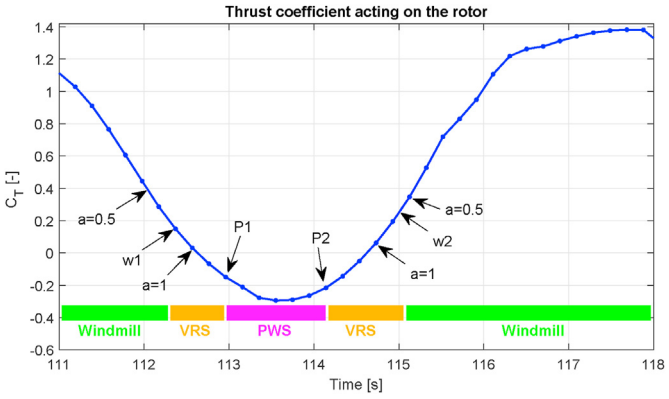

Fig. 22. Thrust coefficient acting on fixed rotor (BS).

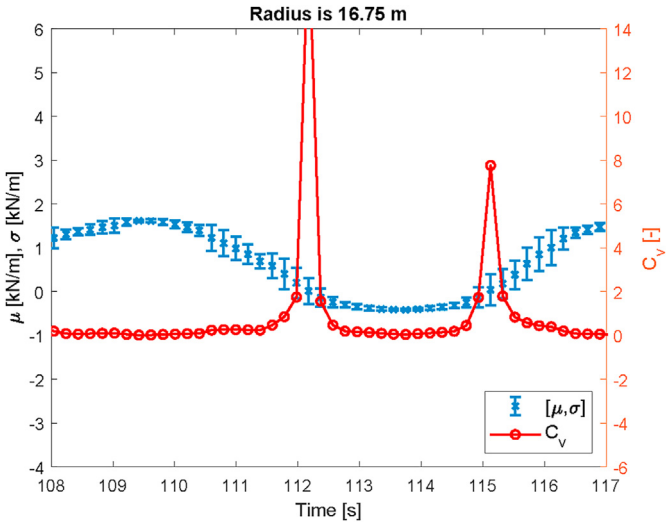

Fig. 23. The μ, σ and C_v of dF_N at r = 16.75 m.

5.5. The aerodynamic load changes corresponding to the working states of the rotor

In order to further investigate the aerodynamics of the FOWT during the change of working state, the time evolution of the

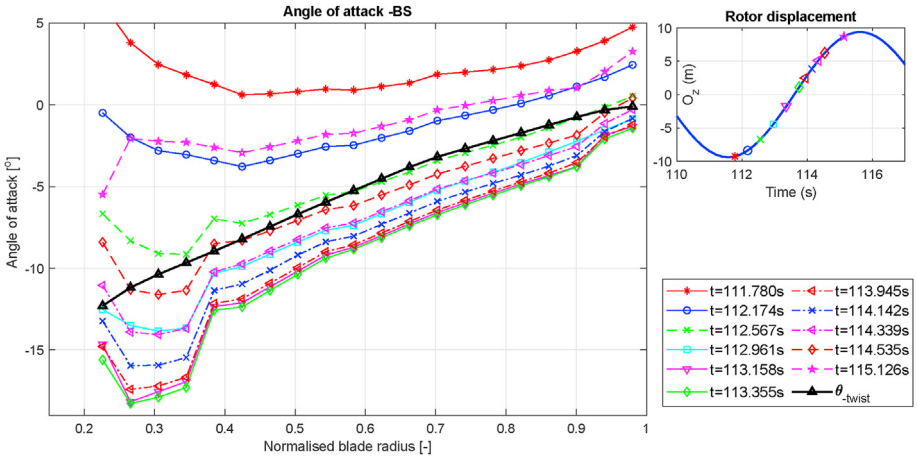

Fig. 21. Angle of attack as a function of the blade radius at different times in the surge cycle (left). The inset in the top right corner shows the surge cycle and visually indicates the location of all time instants in the surge cycle.

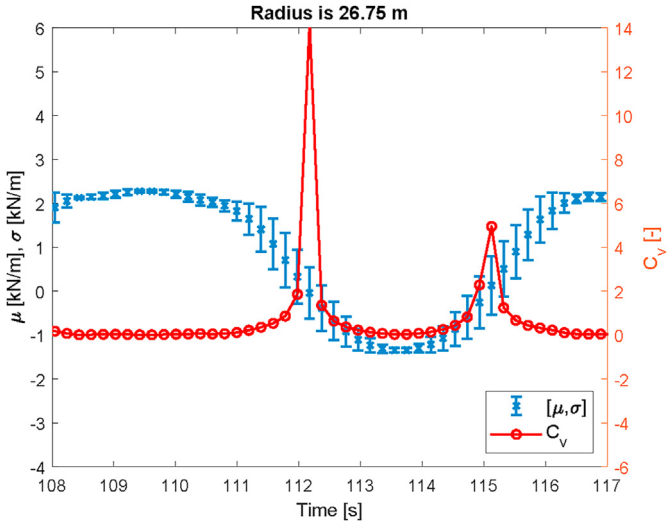

Fig. 24. The μ, σ and C_v of dF_N at r = 26.75 m.

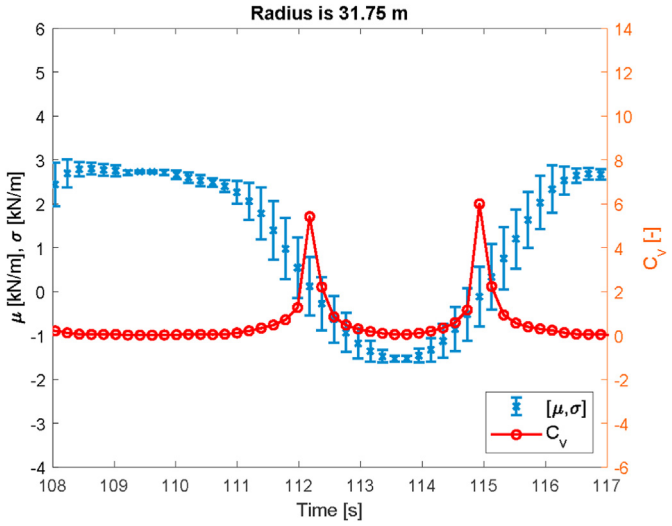

Fig. 25. The μ, σ and C_v of dF_N at r = 31.75 m.

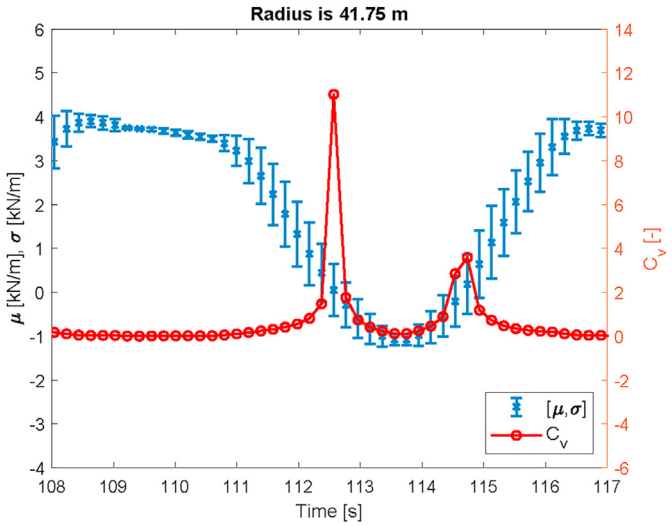

Fig. 26. The μ, σ and C_v of dF_N at r = 41.75 m.

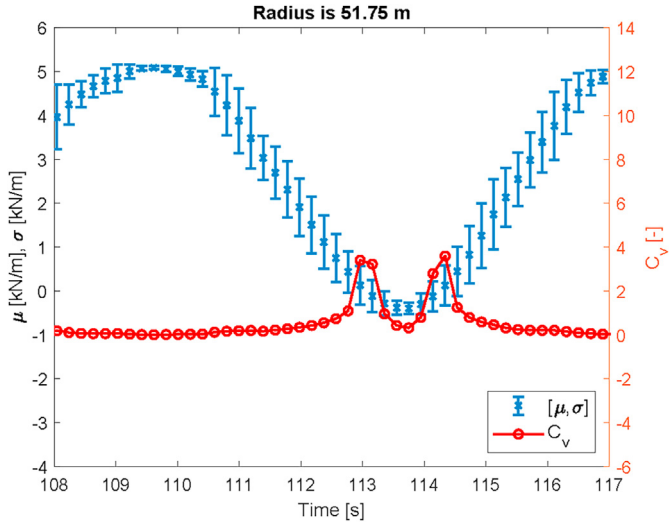

Fig. 27. The μ, σ and C_v of dF_N at r = 51.75 m.

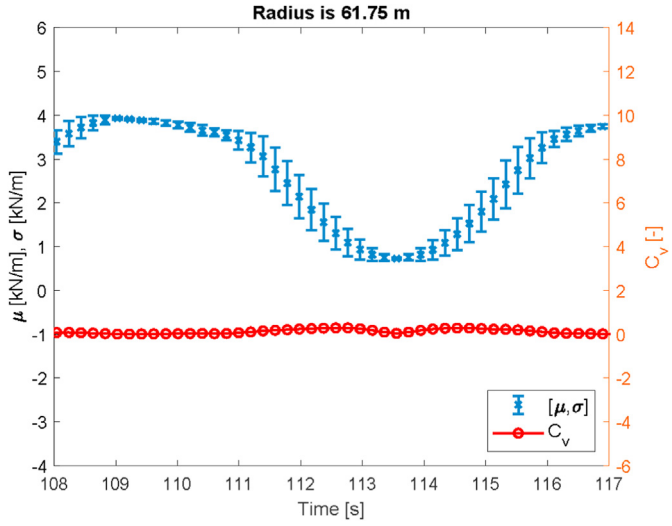

Fig. 28. The μ, σ and C_v of dF_N at r = 61.75 m.

linearized aerodynamic load on blade sections dF_N normal to the rotor disc is shown in Fig. 20, for the load case 'BS'. In order to evaluate the variable dF_N in different aspects, the following parameters are introduced: the mean value μ, standard deviation σ and coefficient of variation C_v, which is defined as

$$C_v = \left|\frac{\sigma}{\mu}\right|. \tag{22}$$

In order to reflect the fluctuations of dF_N in the different working states, in every five consecutive time steps, which is 0.984s, the parameters as introduced above are calculated as:

$$\mu(n_t) = \sum_{i=n_t-2}^{n_t+2} F_n(i), \tag{23}$$

where n_t is the current time step. The surge motion period is 8.1s, which covers about 41 time steps. A pair of vortex rings release to the wake in every 12 time steps. In the paper, the results of an average period of 5 time steps are shown. We also tried to calculate different averaging periods including 3 time steps and 7 time steps. Similar conclusions can be seen. However, the average period

should not be taken too long, because long period results are not accurate enough to represent the local variance of the loads.

From Figs. 23–28, the μ, σ and C_v of dF_N at different blade radius from root to tip are shown in a time span between 108s and 117s, which covers the working states from windmill to propeller. Firstly, as expected, in each figure the mean value μ has its peak value in the windmill working state and its minimum value in the PWS. Also it can be seen that the difference between the maximum and minimum values of μ monotonically increases from r = 16.75 m in Fig. 23 to r = 51.75 m in Fig. 27 and decreases again at the tip (r = 61.75 m) in Fig. 28, while the lowest value of μ occurs in the middle of the blade as shown in Fig. 25. Secondly, in each figure the standard deviation σ changes regularly, i.e., from the region of windmill working state to VRS, σ gradually increases and from the VRS to PWS, σ gradually decreases. Additionally, it can be seen that the maximum value of σ occurs in the middle of the blade in Fig. 25 (in the VRS region). Thirdly, it is found that in each figure the coefficient of variation C_v has two peak values (except on the tip of the blade), both occurring around the VRS boundaries 'w1' and 'w2' as shown in Fig. 22, where μ is close to zero and σ is relatively high. This demonstrates that the fluctuations of the thrust force is significant during the onset of VRS in terms of C_v. It is also seen that from root to tip of the blade, the time interval between the two peak values of C_v decreases, which can be explained with the phenomenon as observed in the flow field around the rotor in Section 5.2. During the working state change from VRS to PWS, the airflow velocity first reverses from inboard of the blade and extends to the outboard of the blade until it is totally directed upwind, which demonstrates the onset of the PWS. When the rotor goes from PWS to VRS, the airflow velocity first reverses from the outboard of the blade and extends to the inboard part, until it returns to a completely downwind orientation corresponding to the windmill working state. Accordingly, during this process, the inboard part of the blade experiences longer time interval of the airflow velocity than the outboard part of the blade, which explains the longer time interval of C_v from inboard of the blade. Finally, C_v in both the windmill working state and the PWS is very small.

6. Conclusion and outlook

In this paper, an in-house code of free wake vortex ring method is used to simulate the aerodynamic performance of the 5 MW NREL floating offshore wind turbine undergoing a prescribed surge motion. The study investigates several characteristics of the rotor during the status switch between different working states.

Firstly, the vortex ring state boundary of the rotor is predicted using both the Wolkovitch criterion and the axial induction factor. The predicted time slots of different working states are taken as a reference of the analysis later in the paper. Then, three different working states are identified visually from the streamlines in the velocity field, which show good correlation with the predicted time slots. Next, the thrust coefficient curve corresponding to these three working states is also analyzed, which shows that the boundaries between different working states are distributed symmetrically along the curve during one cycle of the platform motion. Furthermore, the boundary between the vortex ring state and the propeller working state is identified by comparing the angle of attack with the twist angle of the blade, which provides a new option to numerically distinguish these two working states. Finally, the load analysis are done and it is found that the largest load fluctuations occur at the vortex ring state boundaries (according to Wolkovitch criterion), while the fluctuations of the thrust are less significant in the windmill working state and the propeller working state.

In this paper, the aerodynamic performance of the rotor during a change of working state is discussed in depth. However, this study is limited to a surge motion. Future work should look at other motions, such as a pitch motion and a combination of multiple degrees of freedom. Also, it would be worth discussing ways to mitigate the negative effects of the associated working state changes, considering that the vortex ring state causes large load fluctuations on the rotor and the propeller working state leads to a loss in efficiency. Finally, higher fidelity models should be used to further investigate if such motions do lead to the occurrence of the turbulent wake state.

CRediT authorship contribution statement

Jing Dong: Conceptualization, Methodology, Software, Validation, Formal analysis, Investigation, Resources, Data curation, Writing – original draft, Writing – review & editing, Visualization, Project administration, Funding acquisition. **Axelle Viré:** Writing – review & editing, Supervision.

Declaration of competing interest

The authors declare that they have no known competing financial interests or personal relationships that could have appeared to influence the work reported in this paper.

Acknowledgements

Dong would like to acknowledge support from China Scholarship Council (CSC). We would like to thank Prof. Carlos Simao Ferreira for his participation in the discussion about this research and for sharing his knowledge and experience with us. Special thanks are also given to Jason Jonkman of NREL for his valuable explanation of using FAST. Many thanks to Dr. Zhangrui Li for his technical support in the postprocessing of the data. We also express our sincere gratitude to Ryan Kyle for taking the time to elaborate on his research with us.

References

[1] T. Sebastian, M. Lackner, Characterization of the unsteady aerodynamics of offshore floating wind turbines, Wind Energy 16 (3) (2013) 339–352, https://doi.org/10.1002/we.545.
[2] J. Leishman, Principles of Helicopter Aerodynamics, Cambridge University Press, Cambridge, 2006.
[3] R. Kyle, Y.C. Lee, W.-G. Früh, Propeller and vortex ring state for floating offshore wind turbines during surge, Renew. Energy 155 (2020) 645–657, https://doi.org/10.1016/j.renene.2020.03.105. URL, http://www.sciencedirect.com/science/article/pii/S0960148120304377.
[4] J. Dong, A. Viré, Predicting the occurrence of the vortex ring state for floating offshore wind turbines, J. Phys. Conf. 1618. doi:10.1088/1742-6596/1618/5/052044.
[5] J. Dong, A. Viré, Comparative analysis of different criteria for the prediction of vortex ring state of floating offshore wind turbines, Renew. Energy 163 (2021) 882–909, https://doi.org/10.1016/j.renene.2020.08.027.
[6] J. Dong, A. Viré, Z. Li, Analysis the vortex ring state and propeller state of floating offshore wind turbines and verification of their prediction criteria by comparing with a cfd model, Renew. Energy 184 (2022) 15–25, https://doi.org/10.1016/j.renene.2021.11.053.
[7] T. Sebastian, M. Lackner, Analysis of the induction and wake evolution of an offshore floating wind turbine, Energies 5 (2012) 968–1000, https://doi.org/10.3390/en5040968.
[8] H. Lee, D.-J. Lee, Effects of platform motions on aerodynamic performance and unsteady wake evolution of a floating offshore wind turbine, Renew. Energy 143 (2019) 9–23, https://doi.org/10.1016/j.renene.2019.04.134. URL, http://www.sciencedirect.com/science/article/pii/S0960148119306184.
[9] A. Afjeh, Wake Effects on the Aerodynamic Performance of Horizontal axis Wind Turbines, Tech. rep., NASA contractor report, 09 1984.
[10] J. de Vaal, M. Hansen, T. Moan, Influence of rigid body motions on rotor induced velocities and aerodynamic loads of a floating horizontal axis wind turbine, ASME. International Conference on Offshore Mechanics and Arctic Engineering 9B: Ocean Renewable Energy. doi:10.1115/OMAE2014-24227.
[11] J. Dong, A. Viré, C. Ferreira, Z. Li, G. Van Bussel, A modified free wake vortex ring method for horizontal-axiswind turbines, Energies 12 (20). doi:10.3390/en12203900.

[12] M. Jeon, S. Lee, S. Lee, Unsteady aerodynamics of offshore floating wind turbines in platform pitching motion using vortex lattice method, Renew. Energy 65 (2–3) (2014) 207–212, https://doi.org/10.1016/j.renene.2013.09.009.
[13] T. Tran, D. Kim, The platform pitching motion of floating offshore wind turbine: a preliminary unsteady aerodynamic analysis, J. Wind Eng. Ind. Aerod. 142 (C9) (2015) 65–81, https://doi.org/10.1016/j.jweia.2015.03.009.
[14] T. Tran, D. Kim, J. Song, Computational fluid dynamic analysis of a floating offshore wind turbine experiencing platform pitching motion, Energies 7 (8) (2014) 5011–5026, https://doi.org/10.3390/en7085011.
[15] J. Wolkovitch, Analytical prediction of vortex-ring boundaries for helicopter in steep descents, J. Am. Helicopter Soc. 17 (1972) 13–19, https://doi.org/10.4050/JAHS.17.13.
[16] D. Peters, S. Chen, Momentum theory, dynamic inflow, and the vortex-ring state, J. Am. Helicopter Soc. 27 (3) (1982) 18–24, https://doi.org/10.4050/JAHS.27.18.
[17] A. Leonard, Computing three-dimensional incompressible flows with vortex elements, Annu. Rev. Fluid Mech. 17 (1) (1985) 523–559, https://doi.org/10.1146/annurev.fl.17.010185.002515.
[18] S. Newman, The Induced Velocity of a Vortex Ring Filament, AFM Technical Reports 11/03, University of Southampton, School of Engineering Sciences, 2011.
[19] S. Yoon, S. Heister, Analytical formulas for the velocity field induced by an infinitely thin vortex ring, Int. J. Numer. Methods Fluid. 44 (2004) 665–672, https://doi.org/10.1002/fld.666.
[20] J. Jonkman, S. Butterfield, W. Musial, G. Scott, Definition of a 5-mw Reference Wind Turbine for Offshore System Development, Tech. rep., NREL, 2009.